Proceedings of ISFOG 2025
5TH INTERNATIONAL SYMPOSIUM ON
FRONTIERS IN OFFSHORE GEOTECHNICS
Nantes, France | June 9-13 2025

ISBN 978-2-85782-758-0

Prediction of Uplift Capacity of Deep Horizontal Circular Plate Anchors

Gopika Rajagopal*
Indian Institute of Technology Palakkad, Kerala, India

Sudheesh Thiyyakkandi
Indian Institute of Technology Palakkad, Kerala, India

**gopika795@gmail.com*

ABSTRACT: Anchors are widely employed to resist tensile loads from structures such as transmission towers, tall chimneys, offshore structures, etc. Several factors, including soil properties, embedment depth, and the shape and size of the anchor plate, influence the uplift response. Failure mechanism around the anchor plate can be categorized as shallow and deep based on the embedment depth to plate diameter ratio. Many approaches based on different slip surfaces exist for estimating the uplift capacity of shallow anchors; however, the prediction methods are limited in the case of deep anchors. This study thus proposes an analytical solution to estimate the uplift resistance of deep anchors through a limit equilibrium approach.

The ultimate uplift capacity of the anchor includes the uplift skin resistance of the shaft and the base plate and the uplift bearing resistance of the plate. The magnitude of uplift skin resistance of the shaft and base plate will generally be very small compared to the bearing resistance. Bearing resistance offered by the base of the anchor is predicted by assuming a peach-shaped logarithmic spiral slip surface model. A small wedge of soil is considered inside the slip surface, with the assumption that all external forces acting on this wedge are in a state of equilibrium. The predictability of this approach depends on the initial radius of the logarithmic spiral considered and is correlated to the diameter of the base using an initial radius factor. The proposed solution is found to be in good agreement with the published experimental results.

Keywords: Plate Anchors; Limit Equilibrium Analysis; Uplift Capacity; Deep Failure Mode

1 INTRODUCTION

Plate anchors have become increasingly popular in offshore engineering due to their reliability, ease of installation, and ability to resist significant uplift and lateral forces. Offshore structures, such as floating platforms, wind turbines, mooring systems, and subsea pipelines, are constantly subjected to dynamic forces from waves, currents, and wind. The anchors provide passive resistance to the tensile loads by mobilizing the surrounding soil volume enclosed by the plate (Murray and Geddes, 1987). Depending on the loading direction and the type of structure, plate anchors can be installed horizontally, vertically, or at an inclination. The installation procedure for a horizontal plate anchor involves excavating the ground to the required depth, placing the anchor, and backfilling the soil (Merifield and Sloan, 2006). An anchor is classified as shallow or deep based on the failure mode, which is determined by the embedment depth (H) to plate diameter (D_p) ratio. In a shallow failure mode, the failure surface extends to the ground surface, whereas in a deep failure mode, failure is characterized by localized shear around the anchor and is unaffected by the soil surface location (Merifield, 2011; Tilak and Samadhiya, 2021). Recently, Hu et al. (2023) provided a comprehensive review of critical embedment depth ratios proposed by various authors, as presented in Table 1. Several experimental studies have been conducted on horizontal plate anchors. These studies found that uplift capacity increases with the increase in embedment depth, size of anchor plate, number of plates, and soil density (Das and Seeley, 1975; Ilamparuthi et al., 2002; Liu et al., 2012; Tilak and Samadhiya, 2021; Roy et al. 2021b; Hu et al. 2023).

Table 1. Critical embedment depth ratios (After Hu et al. 2023).

Literature	Shallow anchor	Deep anchor	Relative density
Zhao et al. (2010)	$H/D_p \leq$ 4-6		loose
	$H/D_p \leq$ 7-9		dense
Mittal and Mukherjee (2013)	$H/D_p \leq 6$	$H/D_p \geq 8$	

Zhang (2014)	$H/D_p \leq 2$		loose
	$H/D_p \leq 4$		medium dense
	$H/D_p \leq 5$		dense
Hao et al. (2015)		$H/D_p \geq 6$	medium dense
		$H/D_p \geq 7.5$	dense
Giampa et al. (2019)	$H/D_p \leq 5$		loose, medium dense
Tilak and Samadhiya (2021)	$H/D_p \leq$ 4-6		medium dense

There are several theoretical approaches for estimating the uplift capacity of anchors, each based on different slip surface assumptions. Majer (1955) proposed a vertical slip surface model, where the uplift resistance was calculated as the sum of frictional resistance along the slip surface and the weight of the overlying soil. Later, Mors (1959) assumed a truncated cone model, starting from the base plate and extending to the surface; however, this model was found to overpredict the capacity of deep anchors. Clemence and Veesaert (1977) proposed a similar model, but for anchors with $H/D_p > 5$, the failure surface extended only $2D_p$ to $3D_p$ from the base. Balla (1961) introduced a simplified circular arc model, which was later supported by Baker and Kondner (1966) for anchors with $H/D_p < 6$.

A limit equilibrium-based solution for predicting the uplift capacity of pipelines and strip anchors was proposed by White et al. (2008), assuming an inverted trapezoidal failure block with shear planes inclined at the angle of dilation. Their study was validated against a dataset of 115 model tests on buried pipelines and strip anchors at various embedment depths. Later, experimental tests on pipes and strip plate anchors in sand conducted by Zhuang et al. (2021) identified two distinct failure mechanisms: a wedge-type (general shear) failure and a flow-type (local shear) failure, depending on the relative density and embedment depth ratio. Their findings indicated that for strip anchors in medium-dense sand, a flow-type failure mechanism occurred at an embedment depth ratio (H/D_p) of 7, while an H/D_p of 5 exhibited characteristics of a transitional phase between the two failure modes.

Roy et al. (2021a, 2021b) investigated the uplift response of horizontal plate anchors in sand at shallow depths ($H/D_p \leq 4$) through numerical analyses using a bounding surface plasticity model and experimental studies via centrifuge tests. Furthermore, their study proposed a modified limit equilibrium solution, assuming a rigid block failure mechanism extending to the soil surface, based on finite element (*FE*) results. More recently, Kurniadi et al. (2025) examined the pullout behavior of horizontal circular plate anchors in sand (H/D_p = 3) under varying drainage conditions using *ABAQUS*. Their study found that for non-dimensional uplift velocities (V) between 0.005 and 0.1, the soil remained in a fully drained state. However, as V exceeded 0.1, both the anchor capacity factor and negative excess pore pressure increased, indicating a transition from drained to partially drained conditions.

The peak uplift capacity (P) was commonly correlated with a dimensionless breakout factor (N_{qf}), as defined in Eq. 1. Several empirical equations and design charts have been developed for N_{qf} relating to embedment depth ratios, based on experimental results (White et al. 2008; Ilamparuthi et al., 2002; Liu et al., 2012; Kurniadi et al. 2025).

$$N_{qf} = \frac{P}{\gamma'_s AH} \quad (1)$$

where, γ'_s is the effective unit weight of soil, A is the area of the anchor plate, and H is the embedment depth.

Despite the availability of numerous theoretical models for shallow anchors, predictive approaches for deep circular anchors remain limited, emphasizing the need for further research in this area. This study presents a semi-analytical method to predict the uplift capacity of deep horizontal circular plate anchors using a limit equilibrium approach, incorporating a logarithmic spiral slip surface model for derivation. The proposed prediction method is further validated through comparison with experimental results available in the literature.

2 PROBLEM STATEMENT

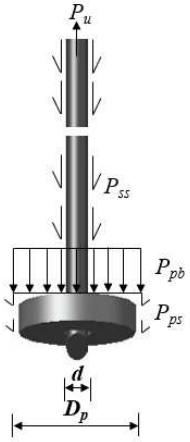

Figure 1. Problem statement.

Figure 1 shows the general schematic diagram of the problem to be analyzed. The ultimate uplift capacity of the anchor (P_u) can be calculated using Eq. 2:

$$P_u = P_{ss} + P_{ps} + P_{pb} \quad (2)$$

where, P_{ss} is the uplift skin resistance of the shaft; P_{ps} is the uplift skin resistance of the plate; and P_{pb} is the uplift bearing resistance of the plate. The magnitudes of P_{ss} and P_{ps} are generally very small compared to P_{pb}, and they can be estimated using conventional methods for predicting skin friction.

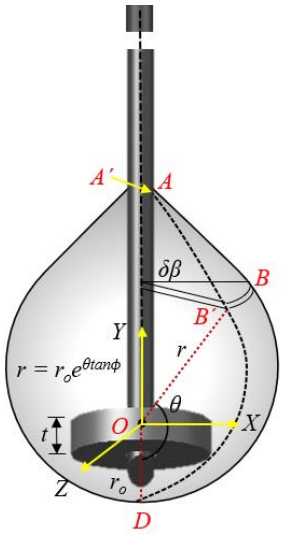

Figure 2. Logarithmic-spiral slip surface model.

The prediction of bearing resistance is a little complex. Previous studies on deep anchors have identified a balloon-shaped failure surface confined within the sand bed under uplift loading (Ilamparuthi and Muthukrishnaiah, 1999; Ilamparuthi et al., 2002; Tilak and Samadhiya, 2021; Hu et al. 2023). In this study, bearing resistance is calculated by assuming a peach-shaped logarithmic-spiral slip surface model with a center at the middle of the plate and radius, r (Eq. 3), as shown in Fig. 2.

$$r = r_o e^{\theta \tan \phi} \quad (3)$$

where, r_o is the initial radius, θ is the angle between the initial radius and line joining any point on the logarithmic-spiral, and ϕ is the angle of internal friction. Xu et al. (2009, 2012) utilized a similar failure surface in their predictions of the uplift capacity of enlarged base piles.

3 PREDICTION OF UPLIFT BEARING RESISTANCE

The limit equilibrium approach was employed to derive the bearing resistance expression, based on the assumption that the moment of all external force components about point *'O'* is zero. As discussed earlier, deep anchors in cohesionless soil may develop a failure surface resembling a log spiral, indicating an inherent rotational tendency in the soil mass. To better capture this behavior, moment equilibrium is incorporated into the analysis. Additionally, this study considers a failure mechanism in which shear stresses are non-uniformly distributed along the failure surface. Accounting for this variation through moment equilibrium provides a more comprehensive representation, as it may not be fully captured using force equilibrium alone.

To estimate the bearing resistance, a small wedge-shaped soil volume, defined by an angle $\delta\beta$, ($ABDB'A'$) is considered (Fig. 2). The forces acting on this wedged soil volume include, (a) shear resistance along the anchor-soil interface; (b) forces along the logarithmic spiral slip surface; and (c) the weight of the soil within the wedged volume. Note that, all the counterclockwise moments were considered positive in the derivation.

3.1 Forces at Anchor-Soil Interfaces

Consider a section of the plate anchor within the wedged volume, with the normal and shear forces acting along the anchor-soil interfaces illustrated in Fig. 3.

Now, the moment due to the forces acting at the shaft-soil interface about 'O' is given by Eq. 4.

$$M_s = -k_o \sigma_v A_{sw} \times \left(\frac{l}{2} + \frac{t}{4}\right) + (\alpha c + k_o \sigma_v \tan \delta) A_{sw} \times \frac{d}{2} \quad (4)$$

where, α is the adhesion factor, c is the cohesion, k_o is the earth pressure coefficient at rest, σ_v is the vertical stress at mid-depth of the anchor, and A_{sw} is the area of the shaft in the wedge (equal to $\frac{d\delta\beta(2l-t)}{4}$).

Similarly, the moment caused by the forces at the plate base-soil interface about point O is given by Eq. 5.

$$M_p = (\alpha c + k_o \sigma_v \tan \delta) A_{pw} \times \frac{D_p}{2} \quad (5)$$

where, A_{pw} is the area of the plate in the wedge (equal to $\frac{D_p \delta\beta t}{2}$).

Now, the moment due to the forces acting at the bearing surface of the plate is (Eq. 6).

$$M_b = \sigma_b A_{bw} \times \frac{D_p}{3} + (\alpha c + \sigma_b \tan\delta) A_{bw} \times \frac{t}{2} \quad (6)$$

where, σ_b is the bearing stress, and A_{bw} is the area of the bearing surface (equal to $\frac{\delta\beta(D_p{}^2 - d^2)}{8}$). Therefore, the total moment due to the forces at the anchor-soil interface can be estimated using Eq. 7.

$$M_1 = M_s + M_p + M_b \quad (7)$$

Upon simplification, M_1 becomes (Eq. 8),

$$M_1 = \frac{-k_o\sigma_v\delta\beta}{16}\left[d\left(4r_o{}^2 e^{2\pi\tan\phi} - t^2\right) - 2d^2\tan\delta\left(2r_o e^{\pi\tan\phi} - t\right) - 4D_p{}^2 t\tan\delta\right] + \frac{\alpha c\delta\beta}{16}\left[2d^2\left(2r_o e^{\pi\tan\phi} - t\right) + 4D_p{}^2 t + \left(D_p{}^2 - d^2\right)t\right] + \frac{\sigma_b\delta\beta}{48}\left[2D_p + 3t\tan\delta\right]\left(D_p{}^2 - d^2\right) \quad (8)$$

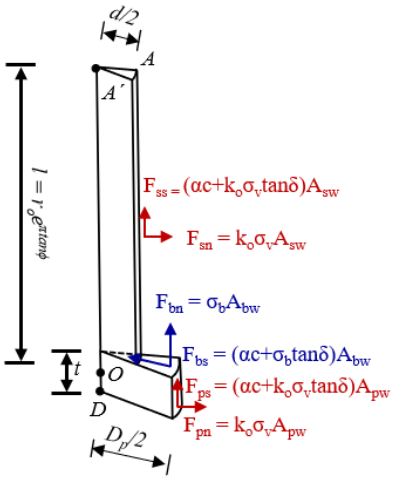

Figure 3. Forces at anchor-soil interface.

3.2 Forces at Logarithmic Spiral Slip Surface

Consider a small area *BEE´B´* (*dA*) on the logarithmic-spiral slip surface (Fig. 4), where the stress state is assumed to follow the Mohr-Coulomb yield criterion (Eq. 9).

$$\tau_n = c + \sigma_n \tan\phi \quad (9)$$

where, σ_n is normal stress and τ_n is shear stress. The shear and normal forces acting on *dA* can be resolved into two components: one along the radial direction and the other perpendicular to it. The moment of all forces acting on *dA* about point *'O'* is simplified and expressed in Eq. 10.

$$dM_2 = -cdA\cos\phi \times r \quad (10)$$

Where, *dA* is given by (Eq. 11),

$$dA = \frac{r^2 \sin\theta\,\delta\beta\,d\theta}{\cos\phi} \quad (11)$$

Now, to obtain the total moment due to the forces at the logarithmic-spiral slip surface, dM_2 is integrated over the entire height of the wedge (*ABEDE´B´A´*) and Eq. 10 becomes,

$$M_2 = -cr_o{}^3\delta\beta\frac{\left(e^{3\pi\tan\phi}+1\right)}{\left(1+9\tan^2\phi\right)} \quad (12)$$

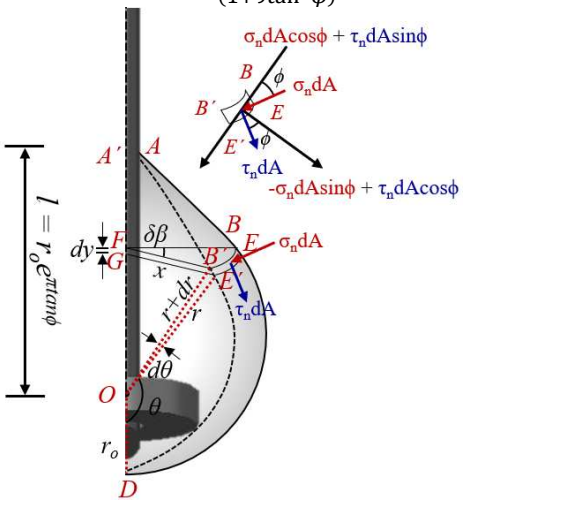

Figure 4. Forces at logarithmic spiral slip surface.

3.3 Weight of Soil in the Wedged Volume

The weight of the soil within the wedge was determined by subtracting the combined weight of the shaft and plate from the total weight of the volumetric wedge (Eq. 13). The wedge was assumed to be fully filled with soil and the weight of the shaft and plate was determined by using the soil's unit weight (γ'_s).

$$W_{soil} = W_{sw} - W_{ss} - W_{sp} \quad (13)$$

where, W_{soil} is the weight of soil in the wedged volume, W_{sw} is the total weight of the wedge, W_{ss} and W_{sp} are the weight of the shaft and plate in the wedge, respectively. Moment due to the weight of each component is calculated by multiplying the respective weight with their lever-arm distance about the point *O*.

To find the total weight of the wedge (W_{sw}), consider a small volume (*dv*) of thickness *dy*, *FBEE´B´G* (Fig. 4), and the weight of this small volume (dW_{sw}) can be calculated using Eq. 14.

$$dW_{sw} = -\gamma'_s dv \quad (14)$$

where, dv is given by (Eq. 15).

$$dv = \frac{r_o{}^3 e^{3\theta \tan\phi} \sin^2\theta(\sin\theta - \tan\phi\cos\theta)}{2} \delta\beta d\theta \quad (15)$$

Now, the moment due to this weight about $'O'$ can be estimated by Eq. 16.

$$dM_{sw} = -\gamma'_s dv \times \frac{2}{3}x \quad (16)$$

Therefore, the moment due to the total weight of the wedge (M_{sw}) is obtained by integrating dM_{sw} from 0 to π, as shown in Eq. 17.

$$M_{sw} = -\int_0^{\pi} \gamma'_s dv \times \frac{2}{3}x = -\frac{\gamma'_s r_o{}^4 \delta\beta\left(e^{4\pi\tan\phi} - 1\right)}{32\tan\phi(1+4\tan^2\phi)} \quad (17)$$

Similarly, the moments due to the weight of the shaft (M_{ss}) and the base plate (M_{sp}) are given in Eq. 18 and Eq. 19, respectively.

$$M_{ss} = -\frac{\gamma'_s d^3 \delta\beta\left(2r_o e^{\pi\tan\phi} - t\right)}{48} \quad (18)$$

$$M_{sp} = -\frac{\gamma'_s D_p{}^3 \delta\beta t}{24} \quad (19)$$

Using Eq. 13, the moment due to the weight of the soil in the wedge (M_3) can now be determined by Eq. 20.

$$M_3 = M_{sw} - M_{ss} - M_{sp} \quad (20)$$

Upon substitution Eq. 20 becomes,

$$M_3 = -\gamma'_s \delta\beta \left[\frac{r_o{}^4\left(e^{4\pi\tan\phi} - 1\right)}{32\tan\phi(1+4\tan^2\phi)} - \frac{d^3\left(2r_o e^{\pi\tan\phi} - t\right)}{48} - \frac{D_p{}^3 t}{24}\right] \quad (21)$$

3.4 Moment Equilibrium Analysis ($\Sigma M_o = 0$)

As mentioned, the moment of the forces acting at the wedged soil volume about the point $'O'$ would be in equilibrium, i.e., $M_1 + M_2 + M_3 = 0$. After substituting and simplifying, the bearing stress (σ_b) at the base plate in the wedged volume is obtained as (Eq. 22a and Eq. 22b),

$$\sigma_b = c\left\{\frac{48\bar{r}_o{}^3\left(e^{3\pi\tan\phi}+1\right) - a\left(12m^2\bar{r}_o e^{\pi\tan\phi} - 9m^2n + 15n\right)\left(1+9\tan^2\phi\right)}{(2+3n\tan\delta)(1-m^2)(1+9\tan^2\phi)}\right\} + \sigma_v\left\{\frac{k_o\left[12m\bar{r}_o{}^2 e^{2\pi\tan\phi} - 3mn^2 - \tan\delta\left(12m^2\bar{r}_o e^{\pi\tan\phi} - 6m^2n + 12n\right)\right]}{(2+3n\tan\delta)(1-m^2)}\right\} + \frac{(D_p-d)\gamma'_s}{2}\left\{\frac{\frac{3\bar{r}_o{}^4\left(e^{4\pi\tan\phi}-1\right)}{\left(\tan\phi(1+4\tan^2\phi)\right)} - 4m^3\bar{r}_o e^{\pi\tan\phi} - m^3n - 4n}{(2+3n\tan\delta)(1-m^2)(1-m)}\right\} \quad (22a)$$

or

$$\sigma_b = cN_c + \sigma_v N_q + 0.5\left(D_p - d\right)\gamma'_s N_\gamma \quad (22b)$$

where, $\bar{r}_o$ is the initial radius factor ($\bar{r}_o = \frac{r_o}{D_p}$); m and n are geometric parameters ($m = \frac{d}{D_p}$ and $n = \frac{t}{D_p}$); N_c, N_q, and N_γ are the uplift capacity factors for deep horizontal plate anchors (Eq. 23a through Eq. 23c). These factors depend on the soil properties and geometric parameters of the anchor.

$$N_c = \frac{48\bar{r}_o{}^3\left(e^{3\pi\tan\phi}+1\right) - a\left(12m^2\bar{r}_o e^{\pi\tan\phi} - 9m^2n + 15n\right)\left(1+9\tan^2\phi\right)}{(2+3n\tan\delta)(1-m^2)(1+9\tan^2\phi)} \quad (23a)$$

$$N_q = \frac{k_o\left[12m\bar{r}_o{}^2 e^{2\pi\tan\phi} - 3mn^2 - \tan\delta\left(12m^2\bar{r}_o e^{\pi\tan\phi} - 6m^2n + 12n\right)\right]}{(2+3n\tan\delta)(1-m^2)} \quad (23b)$$

$$N_\gamma = \frac{\frac{3\bar{r}_o{}^4\left(e^{4\pi\tan\phi}-1\right)}{\left(\tan\phi(1+4\tan^2\phi)\right)} - 4m^3\bar{r}_o e^{\pi\tan\phi} - m^3n - 4n}{(2+3n\tan\delta)(1-m^2)(1-m)} \quad (23c)$$

The bearing resistance (P_{pb}) against uplift is now expressed as shown in Eq. 24:

$$P_{pb} = \frac{\pi}{4}\left(cN_c + \sigma_v N_q + \frac{(D_p-d)\gamma'_s}{2}N_\gamma\right)\left(D_p{}^2 - d^2\right) \quad (24)$$

4 COMPARISON OF PREDICTED AND MEASURED UPLIFT CAPACITIES

The proposed model was validated using experimental results from existing literature (Ilamparuthi et al., 2002; Mittal and Mukherjee 2012; Hao et al. 2019; Tilak and Samadhiya, 2021; Hu et al. 2023). The predictability of this approach depends on the initial radius (r_o) of the logarithmic spiral curve. Analysis of experimental data using the proposed method indicates that the initial radius factor ($\bar{r}_o$) can be expressed as a function of the embedment depth ratio (H/D_p). Figure 5 shows the variation in the initial radius factor with

different H/D_p ratios, as described by the relationship in Eq. 25.

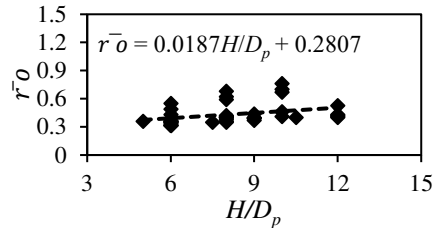

Figure 5. Relationship between initial radius factor and embedment depth ratio.

$$\bar{r_o} = 0.2807 + 0.0187\,\frac{H}{D_p} \qquad (25)$$

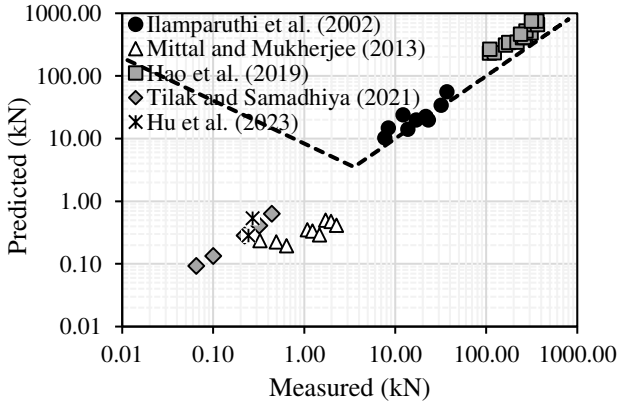

Figure 6. Measured and predicted uplift capacities.

Figure 6 presents a comparison between the measured uplift capacities (P_{um}) of deep circular plate anchors and the predicted capacities (P_u) calculated using the proposed approach. As shown, the predicted pull-out resistance values closely matched the measured capacities. The ratio of predicted to measured capacities (P_u/P_{um}) had a mean of 1.34, based on 41 test samples. To access the applicability of the proposed method, sensitivity analysis was conducted by examining the effect of variation in ϕ and H/D_p on uplift capacity factor, N_q (Fig. 7). As evident, ϕ and H/D_p have a significant impact on N_q, validating the ability of the proposed method to capture key factors affecting deep anchor performance.

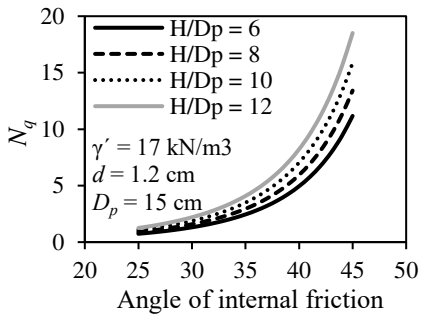

Figure 7. Variation in N_q with ϕ and H/D_p.

5 CONCLUSIONS

This study proposed a limit equilibrium-based prediction method for estimating the uplift resistance of horizontal circular plate anchors under a deep failure mode. A logarithmic spiral slip surface model was utilized to characterize the failure surface accurately. To derive the equation for the bearing resistance provided by the plate, the moment equilibrium of all external forces acting on a small wedge-shaped soil volume along the logarithmic spiral was analyzed. The uplift bearing resistance is expressed in terms of uplift capacity factors, which are influenced by both the soil properties and the geometric parameters of the anchor. The initial radius factor ($\bar{r_o}$) as a function of the embedment depth ratio was also proposed based on existing experimental data. The predicted uplift capacity (P_u) demonstrated good alignment with the measured capacity (P_{um}), with a mean ratio of P_u/P_{um} equals 1.34. The sensitivity analysis highlights the influence of the angle of internal friction and embedment depth ratio on uplift capacity factors, confirming the effectiveness of the proposed method in accurately capturing the impact of key geotechnical parameters on deep anchor performance. However, given the limited number of experimental results available for deep circular plate anchors, further experimental and numerical studies are recommended to validate these findings comprehensively.

AUTHOR CONTRIBUTION STATEMENT

First Author: Formal analysis, Investigation, Resources, Data curation, Validation, Visualization, Writing – Original draft. **Second Author**.: Conceptualization, Funding acquisition, Methodology, Project administration, Supervision, Writing – review & editing.

ACKNOWLEDGEMENTS

The financial support provided to the first author by the Ministry of Education, India, through the Prime Minister's Research Fellowship (*PMRF*) for the completion of this work is gratefully acknowledged.

REFERENCES

Baker, W.H. and Konder, R.L. (1966). Pullout load capacity of a circular earth anchor buried in sand. Highway Research Record, (108).

Balla, A. (1961). The resistance to breaking out of mushroom foundation. Budapest: Hungary.

Clemence, S.P. and Veesaert, C.J. (1977). Dynamic pullout resistance of anchors in sand. In Int Symp on Soil Struct Interaction.

Das, B.M. and Seeley, G.R. (1975). Breakout resistance of shallow horizontal anchors. Journal of the Geotechnical Engineering Division, 101(9), pp.999-1003. https://doi.org/10.1061/AJGEB6.000020

Giampa, J.R., Bradshaw, A.S., Gerkus, H., Gilbert, R.B., Gavin, K.G. and Sivakumar, V. (2019). The effect of shape on the pull-out capacity of shallow plate anchors in sand. Géotechnique, 69(4), pp.355-363.

Hao, D.X., Fu, S.N., Chen, R., Zhang, Y. and Hou, L. (2015). Experimental investigation of uplift behavior of anchors and estimation of uplift capacity in sands. Chinese Journal of Geotechnical Engineering, 37(11), pp.2101-2106.

Hu, W., Lin, Z., Wang, H., Zhao, P., Hao, D. and Gong, J. (2023). Method for calculating the uplift capacity of a circular anchor plate at arbitrary depth in sand. Ocean Engineering, 286, pp.115441.

Ilamparuthi, K., Dickin, E.A. and Muthukrisnaiah, K. (2002). Experimental investigation of the uplift behaviour of circular plate anchors embedded in sand. Canadian Geotechnical Journal, 39(3), pp.648-664. https://doi.org/10.1139/t02-005

Ilamparuthi, K. and Muthukrishnaiah, K. (1999). Anchors in sand bed: delineation of rupture surface. Ocean Engineering, 26(12), pp.1249-1273. https://doi.org/10.1016/S0029-8018(98)00034-1

Kurniadi, R., Roy, A., Maitra, S., Chow, S.H. and Cassidy, M.J. (2025). Uplift mechanism of horizontal circular plate anchors under varying drainage conditions in sand. Computers and Geotechnics, 180, p.107062.

Liu, J., Liu, M. and Zhu, Z. (2012). Sand deformation around an uplift plate anchor. Journal of Geotechnical and Geoenvironmental Engineering, 138(6), pp.728-737. https://doi.org/10.1061/(ASCE)GT.1943-5606.0000633

Majer, J. (1955). Zur berechnung von zugfundamenten. Osterreichische Bauzeitschrift, 10(5), pp.85-90.

Merifield, R.S., (2011). Ultimate uplift capacity of multiplate helical type anchors in clay. Journal of geotechnical and geoenvironmental engineering, 137(7), pp.704-716. https://doi.org/10.1061/(ASCE)GT.1943-5606.0000478

Merifield, R.S. and Sloan, S.W. (2006). The ultimate pullout capacity of anchors in frictional soils. Canadian geotechnical journal, 43(8), pp.852-868. https://doi.org/10.1139/t06-052

Mittal, S. and Mukherjee, S. (2013). Vertical uplift capacity of a group of helical screw anchors in sand. Indian Geotechnical Journal, 43, pp.238-250.

Mors, H., 1959. The behaviour of mast foundations subjected to tensile forces. Bautechnik, 36(10), pp.367-378.

Murray, E.J. and Geddes, J.D. (1987). Uplift of anchor plates in sand. Journal of Geotechnical Engineering, 113(3), pp.202-215. https://doi.org/10.1061/(ASCE)0733-9410(1987)113:3(202)

Roy, A., Chow, S.H., O'Loughlin, C.D., Randolph, M.F. and Whyte, S. (2021). Use of a bounding surface model in predicting element tests and capacity in boundary value problems. Canadian Geotechnical Journal, 58(6), pp.782-799.

Roy, A., Chow, S.H., O'Loughlin, C.D. and Randolph, M.F. (2021b). Towards a simple and reliable method for calculating uplift capacity of plate anchors in sand. Canadian Geotechnical Journal, 58(9), pp.1314-1333.

Tilak, B.V. and Samadhiya, N.K. (2021). Pullout capacity of multi-plate horizontal anchors in sand: an experimental study. Acta Geotechnica, 16, pp.2851-2875. https://doi.org/10.1007/s11440-021-01173-1

White, D.J., Cheuk, C.Y. and Bolton, M.D. (2008). The uplift resistance of pipes and plate anchors buried in sand. Géotechnique, 58(10), pp.771-779.

Xu, H.F., Yue, Z.Q. and Qian, Q.H. (2009). Predicting uplift resistance of deep piles with enlarged bases. Proceedings of the Institution of Civil Engineers-Geotechnical Engineering, 162(4), pp.225-238. https://doi.org/10.1680/geng.2009.162.4.225

Xu, H.F., Yue, Q.Z. and Qian, Q.H. (2012). Failure model of soil around enlarged base of deep uplift piles. Proceedings of the Institution of Civil Engineers-Geotechnical Engineering, 165(5), pp.275-288. https://doi.org/10.1680/geng.8.00020

Zhang, X., (2014). Experimental analysis of soil deformation around uplifting spiral anchors and theoretical research of uplifting capacity models [D]. Zhengzhou University.

Zhao, L.H., Luo, Q., Li, L., Dan, H.C. and Liu, X. (2010). Ultimate pull-out capacity of strip anchor plates with upper bound theorem. Rock Soil Mech, 31(2), pp.516-522.

Zhuang, P.Z., Yue, H.Y., Song, X.G., Yang, H. and Yu, H.S. (2021). Uplift behavior of pipes and strip plate anchors in sand. Journal of Geotechnical and Geoenvironmental Engineering, 147(11), p.04021126.